PAPER • OPEN ACCESS

Dark state photophysics of nitrogen–vacancy centres in diamond

New Journal of Physics
The open access journal for physics

Dark state photophysics of nitrogen–vacancy centres in diamond

K Y Han[1,3,4], D Wildanger[1,3], E Rittweger[1], J Meijer[2], S Pezzagna[2], S W Hell[1,6] and C Eggeling[1,5,6]

[1] Department of NanoBiophotonics, Max Planck Institute for Biophysical Chemistry, Am Fassberg 11, D-37077 Göttingen, Germany
[2] RUBION and Research Department IS3/HTM, Ruhr-Universität Bochum, D-44780 Bochum, Germany
E-mail: ceggeli@gwdg.de and shell@gwdg.de

New Journal of Physics **14** (2012) 123002 (19pp)
Received 14 September 2012
Published 4 December 2012
Online at http://www.njp.org/
doi:10.1088/1367-2630/14/12/123002

Abstract. Nitrogen–vacancy (NV) colour centres in diamond are attractive fluorescence emitters owing to their unprecedented photostability and superior applicability to spin manipulation and sub-diffraction far-field optical microscopy. However, some applications are limited by the co-occurrence of dark state population and optical excitation. In this paper, we use fluorescence microscopy and correlation spectroscopy on single negatively charged NV centres in type IIa bulk diamond to unravel the population kinetics of a >100 s long-lived dark state. The bright–dark state interconversion rates show a quadratic dependence on the applied laser intensity, which implies that higher excited states are involved. Depopulation of the dark state becomes less effective at wavelengths above 532 nm, resulting in a complete fluorescence switch-off at wavelengths >600 nm. This switch is reversible by the addition of shorter wavelengths. This behaviour can be explained by a model consisting of three dark and three bright states of different excitation levels, with the most efficient interconversion via the respective higher excited states. This model accounts for

[3] These authors equally contributed to this work.
[4] Present address: Department of Physics, University of Illinois at Urbana-Champaign, Urbana, IL 61801, USA.
[5] Present address: Weatherall Institute of Molecular Medicine, University of Oxford, Oxford, UK.
[6] Authors to whom any correspondence should be addressed.

the nonlinear dark state and photoswitching kinetics, as well as for the decrease of the NV's fluorescence lifetime with excitation intensity and the strong dependence of fluorescence emission on excitation intensity. Unfortunately, our data do not give enough insight to allow us to assign the different states to specific electronic states known from the literature. Nevertheless, our observations allowed us to improve the recording of fluorescence images of single NV centres with sub-diffraction spatial resolution but they also have important implications for studying their spin states.

Contents

1. Introduction

Since the first optical detection of single nitrogen–vacancy (NV) centres in diamond [1], their spin and optical properties have been extensively investigated (for a review see, e.g., [2]) and further exploited in magnetometry [3, 4] and quantum information processing [5]. The NV defect site consists of a substitutional nitrogen atom next to a vacancy in diamond (figure 1(a)) [6] and is usually negatively charged (NV^-) [7]. However, it is known that it may also appear in a differently charged state, such as the neutral NV^0 state [6], and its charge can be altered depending on the environment or upon illumination [8–10]. The NV ground and excited (fluorescent) states are triplet states [11] having substates that can be optically initialized and read out [12, 13]. The zero-phonon line of NV^- (simply referred to as NV throughout the text) is located at 637 nm and the resulting fluorescence emission is between 600 and 850 nm [2].

Due to the unlimited photostability as well as intriguing photophysical properties, NV centres have been successfully imaged with sub-diffraction optical resolution in the far field

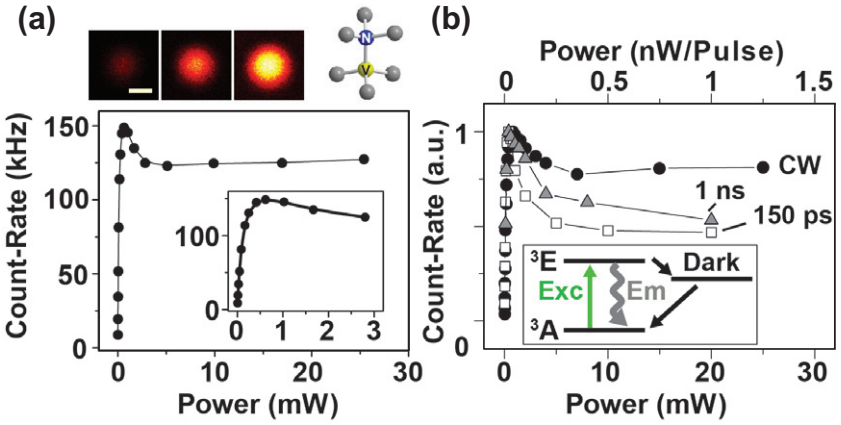

Figure 1. Nonlinear power dependence of NV fluorescence emission. (a) Fluorescence count rate detected for a single NV centre with increasing powers of CW 532 nm light. Insets: (upper left) scanning confocal images of a single NV centre for three different excitation powers (20, 40 and 100 μW), scale bar = 200 nm; (upper right) model structure of an NV centre in diamond; (lower) count rate for powers <3 mW. (b) Fluorescence count rate detected for a single NV centre with increasing powers of CW (black) and pulsed 532 nm light (grey: 1 MHz repetition rate and 1 ns pulse width; open: 20 MHz repetition rate and 150 ps pulse width). Inset: conventional three-state electronic model for NV centre fluorescence emission.

[14, 15] using several mechanisms, including stimulated emission depletion (STED) [16–18], ground-state depletion (GSD) [19, 20] and manipulation of spin orientation [21]. Once the problem of specific staining and functionalization is solved, nanosized diamonds hosting single or multiple NV centres should be very promising as nonbleachable fluorescent markers in cell biology and nanotechnology [22–24].

In spite of the extensive studies that have been performed up to now, many key aspects of the photophysics of the NV fluorescence have remained unclear. Elucidating important details should facilitate overcoming many current limitations of the NV's applicability in quantum information processing [25, 26] and also form the basis of novel far-field nanoscopy variants [19, 20]. Besides the aforementioned ground and excited triplet states, efficient transfer into a metastable dark state has been reported [1, 27, 28]. Based on these observations and when neglecting spin sublevels, the NV centre has been generally modelled as a three-level system consisting of the ground (^{3}A$_2$) and excited (^{3}E) triplet states and a metastable singlet state system with tens of nanoseconds lifetime at room temperature (inset of figure 1(b)) [28]. Strong fluorescence at around 720 nm is detected from ^{3}E, and in this wavelength range the singlet system can be considered dark, albeit emission from the singlet system at around 1050 nm has been proposed [29]. Spin-polarization mechanisms (optical illumination polarizes the NV's spin to an $m_s = 0$ state with $>90\%$) have usually been ascribed to different intersystem crossing rates of each spin state [30, 31]. However, the simple three-level model cannot describe the strongly nonlinear dependence of the fluorescence count rate as well as of the dark state transition rates on the intensity of excitation light [19, 32, 33]. For example, a consistent decrease of the fluorescence count rate for excitation intensities >2 MW cm^{-2} has been observed. Recent work

has further reported on a >100 s long-lived dark state [20] which enables a complete switch-off of the NV's fluorescence by red light, e.g., by exciting into the zero-phonon line [20, 27, 34]; it can be efficiently de-populated by blue light [27]. This state has now been suggested to be NV^0 [25], all in all introducing further complexity into the NV's emission characteristics.

In this paper, we suggest a modified photophysical model for the NV centre's fluorescence emission based on fluorescence microscopy and photon correlation measurements. We demonstrate a resonant two-photon process for dark state population and depopulation, implying that at least three electronic states in the bright triplet and three in a dark state system are involved in these pathways. The wavelength dependence of the population and depopulation kinetics clearly shows a photon energy-dependent bright–dark state equilibrium, explaining the nonlinear dark state and photoswitching characteristics, the decrease of the NV's fluorescence lifetime with excitation intensity and the strongly nonlinear intensity dependence of the fluorescence count rate. Our observations further improve the understanding of this promising emitter and its performance in its different applications. As an example, we show how the photophysical insights helped us to enhance the signal-to-noise ratio in sub-diffraction GSD images of single NV centres.

2. Experimental methods

2.1. Sample

We used several bulk diamonds grown by chemical vapour deposition with a low density of NV centres partly produced by ion beam implantation [35] to detect and image single isolated NV centres.

2.2. Microscope setup for photophysical studies

A custom-built confocal microscope was used to characterize the NV fluorescence [17, 20]. Spatially filtered and collimated excitation beams were reflected by dichroic beamsplitters (AHF Analysentechnik, Tübingen, Germany) and circularly polarized by an achromatic quarter-wave plate (B Halle Nachfl., Berlin, Germany). After focusing the beams onto a single NV centre by an oil immersion objective lens (NA = 1.4, HCX PL APO 100, Leica Microsystems, Wetzlar, Germany), the fluorescence signal was collected by the same objective, spectrally filtered (AHF Analysentechnik) and imaged onto a multimode fibre (M31L01, Thorlabs, Newton, NJ). The fluorescence signal was detected by avalanche photodiodes (SPCM-AQR-13-FC, Perkin-Elmer Optoelectronics, Fremont, CA) and further processed by a multi-channel scaler card (P7882, Fast ComTec, Oberhaching, Germany) for imaging and count-rate observations, a hardware correlator (Flex02-01D, Correlator.com, NJ) for determination of the second-order correlation function $G^{(2)}(t_c)$ of the count-rate fluctuations, or a time-correlated single-photon-counting card (SPC-730, Becker-Hickl, Berlin, Germany) for fluorescence lifetime measurements. The correlation data $G^{(2)}(t_c)$ were measured in a Hanbury Brown–Twiss configuration, where the fluorescence signal incident on a 50 : 50 beamsplitter was imaged onto two avalanche photodiodes. The sample was imaged by scanning a three-dimensional piezo stage (Nano-PDQ375, Mad City Labs, Madison, WI). We used the following continuous-wave (CW) light sources: 473 nm diode laser (FSDL-473-030T, Frankfurt Laser Company, Frankfurt, Germany), 491 nm solid state laser (Calypso 50, Cobolt, Solna, Sweden), 532 nm solid state laser (Verdi 5,

Coherent, Santa Clara, CA), 560 nm fibre laser (VFL-P-1000-560; MPB Communications, Montreal, Canada), 592 nm fibre laser (VFL-P-1000-592, MPB Communications), 638 nm diode laser (PPM-501P, Photonic Products, Gröbenzell, Germany) and a 671 nm solid state laser (SDL-671-300T, Frankfurt Laser Company). For excitation at 600 and 620 nm, we used a 20 MHz pulsed supercontinuum fibre laser (Fianium, Southampton, UK) with a spectral bandwidth of ±5 nm as selected by an appropriate clean-up filter (AHF Analysentechnik). In the case of pulsed excitation we applied 532 nm lasers running at either 20 MHz with 150 ps pulses (Fianium) or at 1 MHz with 1 ns pulses (G1 + Lasersystem, Mobius Photonics, Santa Clara, CA). The 20 MHz laser was further used for the fluorescence lifetime measurements. The illumination times and light intensities were controlled by electro-optic modulators (LM 0202, QiOptiq, formerly Linos, Göttingen, Germany) or acousto-optical filters (MT200-A0.5-VIS, AA Opto-Electronic, Pegasus Optik GmbH, Wallenhorst, Germany) with response times of <20 ns and $<1\,\mu$s, respectively, and with an on–off contrast of >60 dB as specified by the supplier. The temporal synchronization of the different devices was realized by a digital pulse generator (Model 9514+, Scientific Instruments GmbH, Gilching, Germany). Throughout the paper we indicate the power P measured at the sample plane, which corresponds to an intensity $I = P/A$, where $A \approx \pi\ (\mathrm{FWHM}/2)^2$ denotes the focal area with a full-width at half-maximum (FWHM) diameter of the diffraction-limited Gaussian spot. We measured values of FWHM $\approx$ 180–270 nm, i.e. $A \approx 2.5$–5.7×10^{-10} cm^2 for the different 473–671 nm lasers, by scanning over a scattering 80 nm large gold bead (gold colloid, En.GC80, BBinternational) in a nonconfocal mode.

2.3. Ground-state depletion nanoscopy setup

Far-field sub-diffraction GSD imaging of the NV centres was performed on a custom-built setup (figure 3(a)) described in detail previously [19]. Basically, the setup was a confocal microscope where the excitation beam features a doughnut-like intensity distribution. The light of a pulsed laser (532 nm, 20 MHz, Fianium, Southampton, UK) was spatially filtered by a polarization maintaining single-mode fibre (P1-488PM-FC-10, Thorlabs, Newton, NJ). After passing through the fibre, the light was collimated with an achromatic lens ($f = 50$ mm, Linos, Göttingen, Germany) and sent through a phase filter which imprinted a helical phase ramp from 0 to 2π (RPC Photonics, Rochester, NY). Circular polarization is ensured by passing the light through a quarter-wave plate (B Halle Nachfl., Berlin, Germany). A dichroic mirror (DC) reflected the beam into the objective lens (1.46 NA Oil, Leica Microsystems, Wetzlar, Germany) which focused the light into the sample. The fluorescence emitted by the sample was collected by the same objective lens, passed through the dichroic and a detection filter (DF), and is finally focused onto the 62.5 μm core of a multi-mode fibre (M31L01, Thorlabs) which acted as confocal pinhole of 0.3 Airy disc diameter. Finally, the photons were detected by an avalanche photodiode. The diamond sample was moved by a three-dimensional piezo scanning stage (P-733.3DD + E741, Physik Instrumente, Karlsruhe, Germany) with a positioning accuracy of better than 1 nm.

In contrast to most microscopy applications, standard immersion oil could not be used as immersion medium between the lens and the sample because the autofluorescence of the oil generated a large signal which corrupted the signal-to-noise ratio of the recorded images significantly. Therefore 2,2′-thiodiethanol [36] was employed, which even under very hard excitation showed virtually no autofluorescence.

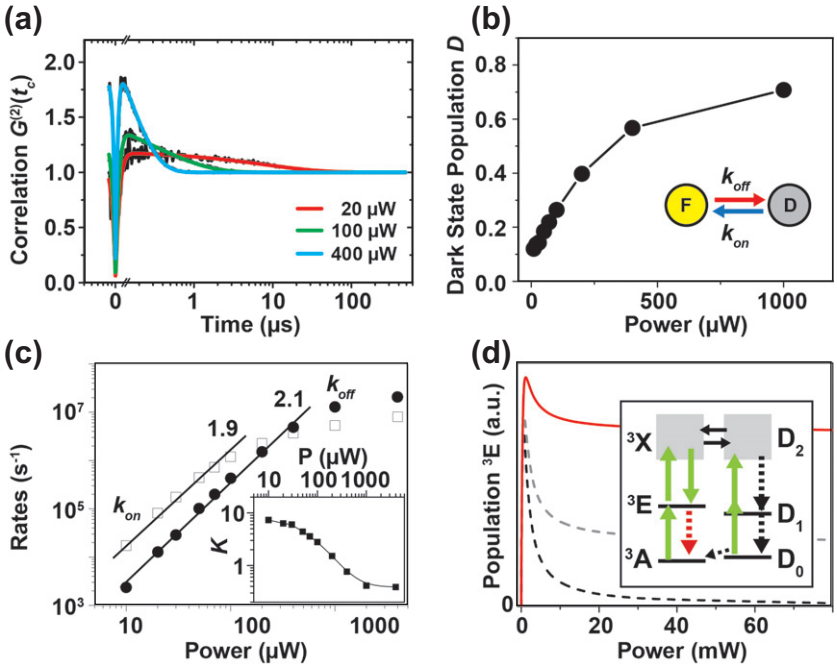

Figure 2. Dark state kinetics of NV centre following CW 532 nm excitation. (a) Representative autocorrelation data $G^{(2)}(t_c)$ for three different excitation powers. (b) Average dark state population D of a single NV centre for different excitation powers determined from $G^{(2)}(t_c)$ using a simplified two-state model (inset) with fluorescent and dark states F and D and interconversion rates k_{off} and k_{on}. (c) Power dependence of k_{off} (black) and k_{on} (open) and of the equilibrium $K = k_{on}/k_{off}$ (inset) determined from $G^{(2)}(t_c)$. The numbers give the power of the dependence. (d) Six-state electronic model of NV fluorescence emission (inset) can theoretically outline the experimentally observed dependence of the count rate, as depicted by the calculated (4) average population of ^{3}E when including stimulated de-excitation of ^{3}X (red line) but not without stimulated de-excitation (black dashed line) or when including excitation to even higher excited electronic states than ^{3}X and D_2 (grey dashed line). Green arrows in the inset indicate excitation, dashed arrows de-excitation with (red) and without (black) emission, and black solid arrows the efficient bright–dark interconversion pathways.

2.4. Correlation analysis

Fluctuations in the fluorescence count-rate time traces were analysed by recording the emission of a single NV centre over time t, $F_1(t)$ and $F_2(t)$, on two single-photon counting detectors in a Hanbury Brown–Twiss configuration, and calculating the cross-correlation function $G^{(2)}(t_c)$ with correlation time t_c:

$$G^{(2)}(t_c) = \frac{\langle \partial F_1(t)\, \partial F_2(t+t_c)\rangle}{\langle F_1(t)\rangle \langle F_2(t)\rangle}, \tag{1}$$

$\delta F = F(t) - \langle F(t)\rangle$ indicates the instant deviation from the time-average signal with the brackets $\langle \ldots \rangle$ denoting averaging of the enclosed arguments over measurement time t. The correlation curves $G^{(2)}(t_c)$ show two characteristic time regions (compare figure 2(a)): a dip at

zero lag times (photon antibunching) stemming from the ground-to-excited state cycling and scaling with the excited state lifetime, and a decay at 0.1–10 μs lag times due to transitions into and out of a dark state, transiently interrupting fluorescence emission (photon bunching) [28, 32]. The ground-to-excited state kinetics (antibunching) are an order of magnitude faster than the dark state transitions (bunching). We therefore treated both kinetics separately and described the correlation data by two exponential terms

$$G^{(2)}(t) \approx 1 - A \exp\,(-t/\tau_{\mathrm{A}}) + B \exp\,(-t/\tau_{\mathrm{B}})\,, \tag{2}$$

where the amplitude A and the rise time τ_{A} characterize the ground-to-excited state kinetics (antibunching), while the amplitude B and decay time τ_{B} correlate with the population and lifetime of the NV's dark state, respectively (bunching). We corrected the registered correlation functions for random background signal from Rayleigh and Raman scattering, as described in [37].

In the correlation analysis, we approximated the bunching kinetics by a simple two-state model with a bright fluorescent state F and a dark state D (inset of figure 2(b)), which allows the calculation of the relative population D of the dark state (i.e. the probability D of populating the dark state D) and the interconversion rates k_{off} and k_{on}:

$$D = \frac{B}{1+B} = \frac{k_{\mathrm{off}}}{k_{\mathrm{on}} + k_{\mathrm{off}}}, \quad \tau_B^{-1} = k_{\mathrm{on}} + k_{\mathrm{off}}. \tag{3}$$

2.5. Modelling the power dependence of the nitrogen–vacancy fluorescence emission

We approximated the dependence of the average fluorescence count rate of the NV centre on the intensity (or power) of the exciting laser by calculating the equilibrium population of the first excited triplet state ^{3}E using the six-state model of figure 2(d) with the underlying rate equation system

$$\begin{aligned}
0 = \frac{\mathrm{d}}{\mathrm{d}t}\begin{pmatrix} {}^3A \\ {}^3E \\ {}^3X \\ D_0 \\ D_1 \\ D_2 \end{pmatrix} &= \begin{pmatrix} -k_{\mathrm{exc}} \\ k_{\mathrm{exc}} \\ 0 \\ 0 \\ 0 \\ 0 \end{pmatrix} {}^3A + \begin{pmatrix} k_{3E-3A} \\ -(k_{3E-3A} + k_{3E-3X} + k_{3E-D1}) \\ k_{3E-3X} \\ 0 \\ k_{3E-D1} \\ 0 \end{pmatrix} {}^3E \\
&+ \begin{pmatrix} 0 \\ k_{3X-3E} \\ -(k_{3X-3E} + k_{3X-D2}) \\ 0 \\ 0 \\ k_{3X-D2} \end{pmatrix} {}^3X + \begin{pmatrix} k_{D0-3A} \\ 0 \\ 0 \\ -(k_{D0-3A} + k_{D0-D1}) \\ k_{D0-D1} \\ 0 \end{pmatrix} D_0 \\
&+ \begin{pmatrix} 0 \\ k_{D1-3E} \\ 0 \\ k_{D1-D0} \\ -(k_{D1-3E} + k_{D1-D0} + k_{D1-D2}) \\ k_{D1-D2} \end{pmatrix} D_1 + \begin{pmatrix} 0 \\ 0 \\ k_{D2-3X} \\ 0 \\ k_{D2-D1} \\ -(k_{D2-3X} + k_{D2-D1}) \end{pmatrix} D_2,
\end{aligned} \tag{4}$$

^3E, ^3A, ^3X, D_0, D_1 and D_2 denote the equilibrium probabilities of populating the ground (^{3}E and D_0), first excited (^{3}A and D_1) and higher excited (^{3}X and D_2) states of the bright and a dark state system, respectively, with $^3E + {}^3A + {}^3X + D_0 + D_1 + D_2 = 1$. The light-dependent rates k_{exc}, k_{3E-3X}, k_{D0-D1} and $k_{D1-D2} = \sigma_N^* I$ for transfer to a higher excited electronic state scale with the excitation intensity I according to the respective factors $\sigma_N^* = \sigma_N \lambda / hc$ (where the index N is an ambiguous letter for the antecedent indices, σ_N is the absorption cross section for excitation at wavelength λ, h is Planck's constant and c is the speed of light. λ/hc is the inverse photon energy of the exciting light). De-excitation to the next lower excited state is given by the rates k_{3E-3A}, k_{3X-3E}, k_{D1-D0} and k_{D2-D1}. Bright-to-dark and dark-to-bright state transfer rates are given by $k_{3\mathrm{E}-D1}$, k_{3X-D2}, k_{D1-3E} and k_{D2-3X}, resulting in respective crossing probabilities $\phi_N = k_N/(k_N + k_{N-1})$ (with indices $N = 3E$–$D1$, $3X$–$D2$, $D1$–$3E$ and $D2$–3X and $N - 1 = 3E$–$3A$, $3X$–$3E$, $D1$–$D0$ and $D2$–$D1$, respectively). In any case the index denotes the respective transition.

We applied the following parameters in our calculations: $\lambda = 532\,\mathrm{nm}$, $\sigma_{\mathrm{exc}} = 1 \times 10^{-17}\,\mathrm{cm}^2$, $\sigma_{3E-3X} = 1 \times 10^{-14}\,\mathrm{cm}^2$, $\sigma_{D0-D1} = 2 \times 10^{-16}\,\mathrm{cm}^2$, $\sigma_{D1-D2} = 2 \times 10^{-15}\,\mathrm{cm}^2$, $k_{3E-3A} = (12\,\mathrm{ns})^{-1}$, $k_{3X-3E} = k_{D1-D0} = k_{D2-D1} = (100\,\mathrm{ps})^{-1}$, $\phi_{3E-D1} = \phi_{D1-3E} \approx 0$, $k_{D0-3A} = (150\,\mathrm{s})^{-1}$, $\phi_{3X-D2} = 10^{-8}$, and $\phi_{D2-3X} = 10^{-6}$. σ_{exc} was taken from the literature [6], $k_{3E-3A} = 1/12.8\,\mathrm{ns}$ was identified with the inverse fluorescence lifetime, k_{3X-3E}, k_{D1-D0} and k_{D2-D1} were approximated, k_{D0-3A} was taken from our previous measurements [20] and σ_{3E-3X}, σ_{D0-D1}, σ_{D1-D2}, ϕ_{3E-D1}, ϕ_{D1-3E}, ϕ_{3X-D2} and ϕ_{D2-3X} were adjusted to best follow the experimentally observed dependence of the fluorescence count rate on the excitation power P. The laser intensity $I = P/(\pi(\mathrm{FWHM}/2)^2)$ was calculated from P using an FWHM = 250 nm of the exciting laser spot. Our goal was not to fully fit the experimental data, but just to get an understanding of what transitions have to be considered to describe the experimentally observed power dependence of the fluorescence count rate. To achieve this, we had to include light-induced (stimulated) de-excitation of ^{3}X: $k_{3X-3E} = (100\,\mathrm{ps})^{-1} + 1.5 \times 10^{-15}\,\mathrm{cm}^2\,(\lambda/hc)\,I$. The inclusion of even higher excited states than ^{3}X and D_2 with additional bright–dark state interconversion pathways did not realize a proper description of the experimental observations (compare figure 2(d)).

3. Results and discussion

3.1. Power dependence of the NV fluorescence count rate

Fluorescence of the NV centre is excitable by green light at around 532 nm generating a bright signal between 600 and 850 nm [1, 6]. Figure 1(a) shows the fluorescence emission rate of a single NV centre in type IIa bulk diamond at room temperature with increasing power of the CW 532 nm excitation light, detected at wavelengths >655 nm and <700 nm (including subtraction of background, for example, from scattering laser light as determined from the signal measured at dark areas of the diamond). The fluorescence emission is saturated at around $P = 0.5\,\mathrm{mW}$ (corresponding to an intensity of $I = 3.1\,\mathrm{MW\,cm^{-2}}$) and the maximum count rate is 1.5×10^5 counts s^{-1}. This saturation behaviour follows from the depletion of the ground state ^{3}A by an increased population of the excited ^{3}E state or metastable dark states, i.e. it can well be modelled by the three-level system (inset of figure 1(b)). However, this simple scheme cannot describe the concomitant decrease of the fluorescence count rate for higher powers, consistent with previous reports [19, 32, 33]. Even more, the count rate saturates again at $P > 3\,\mathrm{mW}$ to a value of

1.25×10^5 count s^{-1}, which is below the maximum of 1.5×10^5 count s^{-1}. Our observations indicate a much more complex model of fluorescence emission with the involvement of more than three NV states.

3.2. Power dependence of the dark state kinetics

We investigated the kinetics of bright-to-dark state transitions by recording second-order photon correlation data $G^{(2)}(t_c)$ (1) from single isolated NV centres for increasing excitation powers P of 532 nm CW laser light (figure 2(a)). Fitting these data simply by two exponentials as in (2) allows an approximation of the probability of populating a dark state system D and of the interconversion rates k_{off} and k_{on} between the bright and dark state systems (3) (inset of figure 2(b)).

Figure 2(b) shows values of the probability D determined from $G^{(2)}(t_c)$ for different excitation powers P. The dark state population strongly increases with P and there is a probability of up to 80% to populate the dark state already at excitation powers as low as 1 mW. Figure 2(c) shows the power dependence of the off- and on-rates k_{off} and k_{on}. We determined both the increase of the dark state population rate k_{off} with P (which is expected, since the population starts from the excited state), as well as of k_{on}, i.e. a decrease of the dark state residence time ($\sim 1/k_{on}$), which indicates light-induced reversing [38]. For $P < 100\,\mu$W both k_{off} and k_{on} increase with P by a power of two, demonstrating two-step absorption processes, i.e. the involvement of even higher excited states. Both rates increase less for $P > 100\,\mu$W, demonstrating the saturation of the excitation into these higher excited states, i.e. the excitation becomes stronger than the de-excitation. This saturation is more pronounced for the on-rate k_{on}. As a consequence, for $P > 0.4$ mW the transitions to the dark state (off) are stronger than out of the dark state (on, $k_{off} > k_{on}$), which is reversed for lower powers ($k_{off} < k_{on}$). In other words, for large powers the equilibrium $K = k_{on}/k_{off}$, which is >7 for low powers, shifts to the dark state $K < 0.4$ (inset of figure 2(c)). This change in orders accounts for the decrease in count rate, which we have observed for $P > 0.4$ mW (figure 1(a)). The levelling off of the count rate for $P > 3$ mW results from the fact that both rates k_{on} and k_{off} are saturated at these powers, i.e. $K = k_{on}/k_{off} < 0.4$ remains constant.

3.3. Electronic state model

As a result of the correlation data, we can set up an electronic state model for the NV fluorescence emission involving six states (figure 2(d)): the ground and first excited (triplet) states ^{3}A and ^{3}E (the latter being the fluorescent state), a further excited triplet state ^{3}X, from where very efficient crossing to a dark state is possible. The dark state is composed of three differently excited states, a ground D_0, a first excited D_1 and a higher excited state D_2. Reverse crossing to the bright triplet state is most efficient from D_2, while thermal relaxation from D_0 to ^{3}A is very slow with a time constant in the range of >100 s, as demonstrated previously [20, 25, 26]. By introducing an absorption cross section of 10^{-17} cm^2 for the ^{3}A to ^{3}E excitation from the literature [6] and a fluorescence lifetime of $\sim$12.8 ns from experiments (compare figure 3), and assuming lifetimes of the other excited states in the range of 100 ps, we can adapt all other parameters (cross sections σ_{3E-3X}, σ_{D0-D1} and σ_{D1-D2} and dark–bright state interconversion probabilities ϕ_{3E-D1}, ϕ_{D1-3E}, ϕ_{3X-D2} and ϕ_{D2-3X} as detailed in section 2.5) to model both the saturation of the fluorescence count rate as well as its decline and levelling off

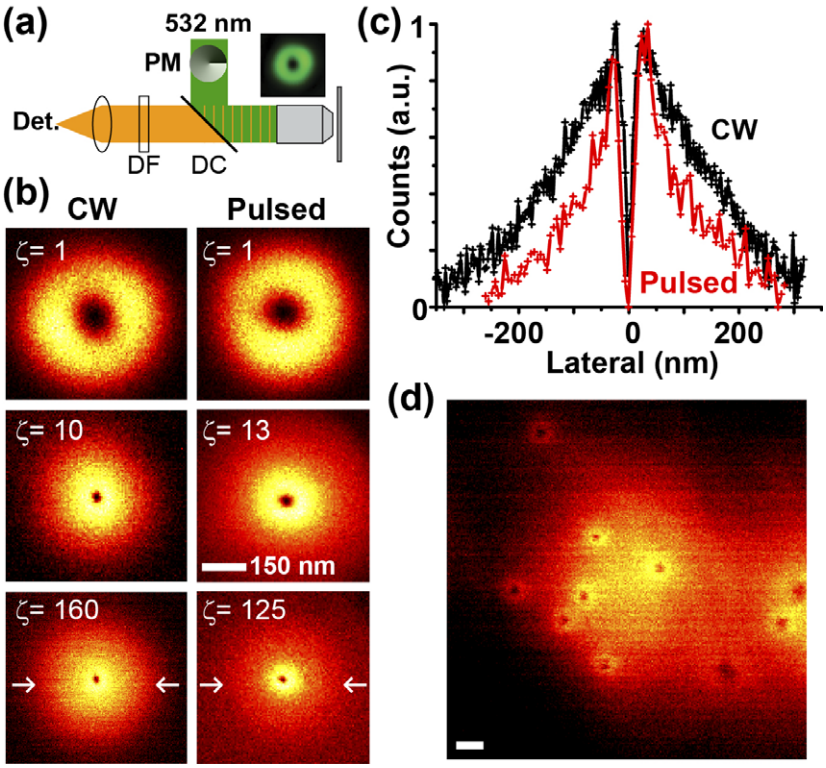

Figure 3. Improved fluorescence GSD nanoscopy on single NV centres in diamond using pulsed (20 MHz, 150 ps) 532 nm light. (a) GSD nanoscope setup with DF, DC, detector (Det.), objective (grey) and excitation (532 nm, green) and fluorescence (orange) light. The intensity distribution of the excitation light is doughnut shaped at the sample (inset) realized by insertion of a phase mask (PM). (b) Fluorescence scanning images of a single NV centre for increasing excitation power $\zeta = P/P_{0.5}$ of CW (left) and pulsed (right) light, where P is the average power and $P_{0.5}$ is the power needed to elicit half of the NV's maximum count rate. (c) Intensity line profiles through the lower images of (b) (as indicated by the arrows), demonstrating an improved SBR for the pulsed excitation modality. (d) Fluorescence scanning GSD nanoscopy image of several NV centres for $\zeta \approx 100$. Scale bar = 200 nm.

towards large excitation powers (figure 2(d)). We have to include light-induced (stimulated) de-excitation of ^{3}X to recover the experimentally observed decline—without stimulation de-excitation, the count-rate would decrease to zero for very large powers. We can safely neglect stimulated fluorescence emission (^{3}E $\rightarrow$ ^{3}A) by the 532 nm light, since emission of NV fluorescence is zero at this wavelength [17]. Note that the inclusion of states further excited than ^{3}X and D_2 cannot recover our observations, resulting as well in a decrease to zero count rate for large powers. Due to the numerous unknown parameters, we cannot give exact values of the involved rate constants and absorption cross sections, or even fit the experimental data. We can only present a model that provides an explanation for the observed power dependence of the NV emission.

3.4. Pulsed excitation

Figure 1(b) shows the dependence of the fluorescence count rate of single NV centres on the average excitation power for pulsed excitation at 532 nm with 1 and 20 MHz repetition rates and pulse widths of 1 ns and 150 ps, respectively. In both cases, we observed similar behaviour as for the CW excitation, confirming our above conclusions: linear dependence for low average powers, saturation to a maximum count rate, decrease for ongoing powers and saturation at very large powers to a value that is below the maximum. However, one main difference between the different excitation modalities becomes obvious: the difference between the maximum count rate and the final saturation level is larger for the pulsed than for the CW excitation and it is largest for the shortest pulse width of 150 ps. Our electronic state model of figure 2(d) can also give an explanation for these observations. It is known that the large peak powers accompanying the pulsed modality lead to a stronger saturation of the optically driven transition (or excitation) to higher electronic state [39, 40]. This 'pulse saturation' is more pronounced for short pulses [39] and also affects the transitions to ^{3}X and D_2, i.e. the interconversion rates k_{on} and k_{off}. Our observations for CW excitation (compare figure 2(c)) showed that the on-switching, i.e. the dark-to-bright interconversion rate k_{on} (and thus excitation to D_2), is more saturated than the off-switching, i.e. the bright-to-dark interconversion rate k_{off} (and thus excitation to ^{3}X). Therefore, it is to be expected that for large peak powers, off-switching (i.e. k_{off}) is favoured. The largest pulse peak powers are provided by excitation with short pulse widths, realizing the most pronounced lowering of the count rate for the 150 ps pulses.

3.5. Improved far-field fluorescence nanoscopy

Far-field fluorescence microscopy is a minimally invasive and very sensitive technique, allowing the quantitative investigation of complex biological objects in the living cell. However, many problems cannot be solved due to the limited spatial resolution of >200 nm imposed by diffraction in standard systems [41]. A remedy to this limit is the photoswitching of fluorescence [42], ensuring that the measured signal stems from a region of the sample that is much smaller than these 200 nm and realizing the transition from microscopy to nanoscopy [15]. Examples are based on STED [14], on the use of photoswitchable fluorescent markers [43, 44] or on the depletion of the fluorescence marker's ground state (GSD) [45, 46]. In an application of the latter concept, the fluorescence emission of NV centres in diamond was excited by a doughnut-shaped focal pattern of 532 nm light featuring a central zero-intensity point [19]. Excitation with large laser powers drove the emission into saturation everywhere except at the focal centre, leaving an area $\ll 200$ nm in diameter, where no fluorescence signal is elicited and which is surrounded by a ring where emission is brightly excited. Scanning of this tiny dark spot over the sample produced a negative image where the NV centres appeared as dark holes on a high fluorescent background, allowing the determination of their spatial distribution with sub-diffraction spatial resolution. A positive image can be derived by deconvolution with the doughnut-shaped emission distribution or by employing a pump–probe scheme [19] (figure 3). A drawback of this imaging scheme is the bright and broad ring around each feature limiting the signal-to-background ratio (SBR) of the final image.

We can use the insights gathered from the power dependence of the NV fluorescence count rate to improve the SBR of the GSD nanoscopy images. Specifically, by using 532 nm pulses instead of CW excitation, we can in the images reduce the extent of the bright ring surrounding

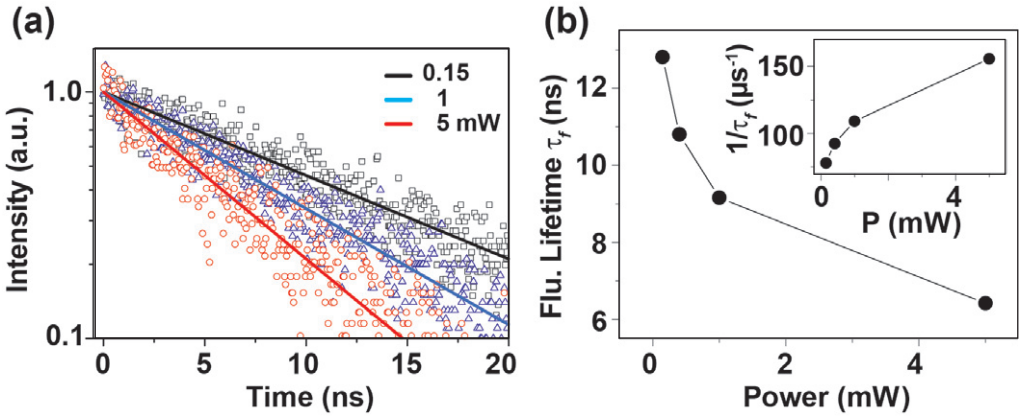

Figure 4. Decrease of the NV fluorescence lifetime for increasing excitation power. (a) Representative fluorescence lifetime decays of a single NV centre for different average powers of pulsed 532 nm excitation (20 MHz, 150 ps). (b) Power dependence of the fluorescence lifetime τ_f and its inverse $1/\tau_f$ (inset).

the dark holes without deteriorating their width. Figure 3 shows the comparative performance of GSD nanoscopy on single NV centres for using a 532 nm CW and a 20 MHz laser with a pulse width of 150 ps for saturated excitation in the doughnut mode. On the one hand, it shows the profiles of the fluorescence intensity emitted from a single isolated NV centre when scanning the doughnut. As expected, the width of the dark central hole is efficiently decreased upon increasing the average excitation power. A measure of the SBR of this nanoscopy modality is given by the ratio of the (almost zero) central intensity and the intensity in the ring, which is much better for the pulsed modality. This is because, for the pulsed modality, the signal count rate drops to $<50\%$ of the maximum value at very high average laser powers, while this drop is only to about 80% for the CW case (figure 1(b))—note that the spatial resolution does not improve, but the improved SBR results in a better contrast. Consequently, scanning a larger area of the diamond with several NV centres using pulsed excitation clearly resolves single close-by NV centres as dark spots.

3.6. Fluorescence lifetime

Our previous observations also have an impact when measuring the fluorescence lifetime of the NV centre. The fluorescence lifetime τ_f of the NV centre involves all depopulation pathways of the ^{3}E state (radiative and nonradiative), i.e. $1/\tau_f = k_{3E-3A} + k_{3E-D1} + k_{3E-3X}$ with k_{3E-3A}, k_{3E-D1} and k_{3E-3X} denoting the rate constants of the $^3\mathrm{E} \rightarrow {}^3\mathrm{A}$ decay, $^3\mathrm{E} \rightarrow \mathrm{D}_1$ crossing and $^3\mathrm{E} \rightarrow {}^3\mathrm{X}$ excitation, respectively. Due to the additional light-driven absorption process, the latter rate k_{3E-3X} increases with excitation power P, so we expect the lifetime τ_f to decrease for strong excitation. Figure 4 shows fluorescence lifetime decays of a single NV centre recorded with the 20 MHz pulsed excitation and time-correlated single-photon counting. The lifetime decreases from 12.8 ns at low P to $\tau_f \approx 6.4$ ns at $P = 5$ mW average power. The increase of $1/\tau_f$ (i.e. the $^3\mathrm{E} \rightarrow {}^3\mathrm{X}$ excitation) saturates at large P, stemming from the saturation of the $^3\mathrm{E} \rightarrow {}^3\mathrm{X}$ excitation.

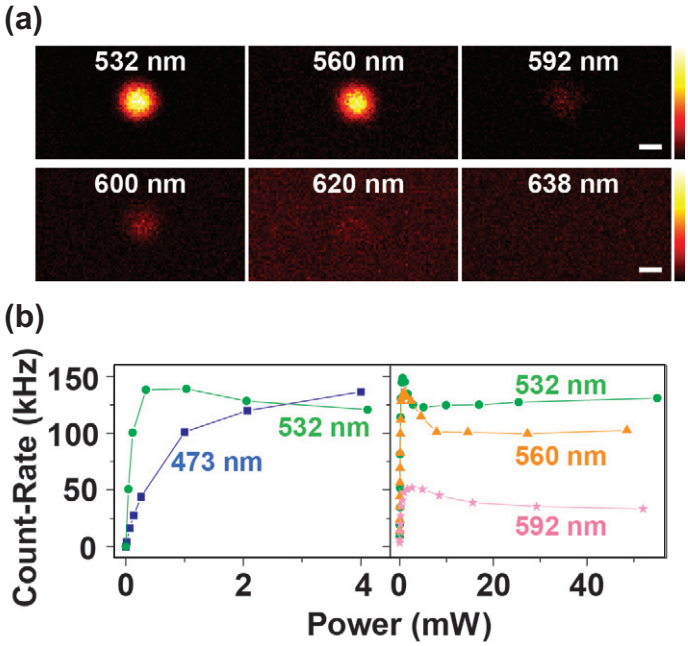

Figure 5. Wavelength dependence of NV fluorescence excitation. (a) Scanning confocal fluorescence images of a single NV centre for 532 (40 μW), 560 (40 μW), 592 (40 μW), 600 (250 μW), 620 (400 μW) and 638 nm (75 μW) excitation. Scale bar: 200 nm. (b) Dependence of fluorescence count rate of single NV centres on the laser power for different excitation wavelengths.

3.7. Wavelength dependence of excitation

We previously used the population of the NV centre's dark state as a photoswitching mechanism for far-field fluorescence nanoscopy [20]. It has repeatedly been reported that the resonant excitation from ^{3}A to ^{3}E at 630–640 nm at room or cryogenic temperatures quickly turns off the fluorescence emission of the NV centre, while addition of blue or green light recovers it by probably depopulating a metastable dark state or charge traps [20, 25–27, 34]. We therefore tested the NV centre's fluorescence emission for different excitation wavelengths of 470–670 nm. This is possible, since the NV centre has a very broad absorption spectrum [6]. Figure 5 shows fluorescence scanning images of a single NV centre and the power dependence of fluorescence emission recorded for different excitation wavelengths. The highest fluorescence yield is acquired at excitation wavelengths $\leqslant$532 nm, increasingly declining for longer wavelengths. As mentioned, illumination at wavelengths close to zero-phonon line or at the long-wavelength tail of the NV's absorption spectrum (620–640 nm) hardly excites fluorescence emission at room temperature at all. At a first glance, this seems to contradict the Kasha–Vavilov rule of conventional fluorophores, which states that the quantum yield of fluorescence is independent of the excitation wavelength [47].

Figure 6 depicts second-order correlation data $G^{(2)}(t_c)$ of the NV fluorescence recorded for different powers P at different wavelengths. Analysis of the data according to (2) and (3) renders the population of the dark state at longer wavelengths much more efficient (figure 6(b)). For example, at 592 nm excitation, the NV centre stays approximately 80% of the time

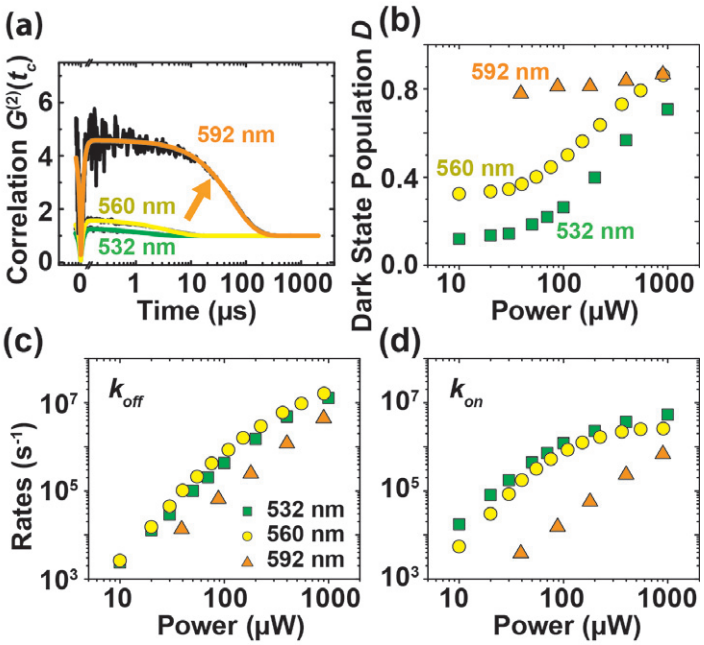

Figure 6. Dependence of the dark state kinetics on the excitation wavelength using fluorescence autocorrelation spectroscopy. (a) Representative autocorrelation data $G^{(2)}(t_c)$ for three different CW excitation wavelengths. The excitation powers were 40 μW for all wavelengths. (b) Average dark state population D of a single NV centre for different CW excitation wavelengths and powers determined from $G^{(2)}(t_c)$. (c), (d) Power dependence of k_{off} (c) and k_{on} (d) determined from $G^{(2)}(t_c)$ for different CW excitation wavelengths, indicating a significantly increased dark state population for the 592 nm excitation (arrow).

in the dark state already at $P < 50\,\mu$W. Interconversion rates k_{off} and k_{on} increase with P with the power of two for all wavelengths. However, while the off-rate k_{off} only slightly decreases towards longer wavelengths, light-induced depopulation of the dark state (k_{on}) is dramatically reduced at longer wavelengths. Consequently, the lower fluorescence yield at longer wavelengths follows from a less efficient depopulation and thus increased population of the NV's dark states. Unfortunately, due to a very bad signal-to-noise ratio we could not accurately analyse correlation data at wavelengths >600 nm.

3.8. Photoswitching of NV fluorescence

As mentioned before [20, 25–27, 34], the negligible fluorescence emission of an NV centre for excitation at wavelengths >600 nm can efficiently be switched on by addition of low levels of 473 or 532 nm light, as can be witnessed in scanning images and in the power dependence of the fluorescence of a single NV centre following 638 nm excitation with and without light of 473 or 532 nm wavelength and $<20\,\mu$W power (figure 7(a)). The relative increase in the maximum achievable fluorescence emission rate upon addition of 473 nm light was largest for wavelengths of around 620–650 nm (figure 7(b)). However, the addition of the 473 nm light did not notably increase the maximum rate obtained for 532 and 560 nm excitation,

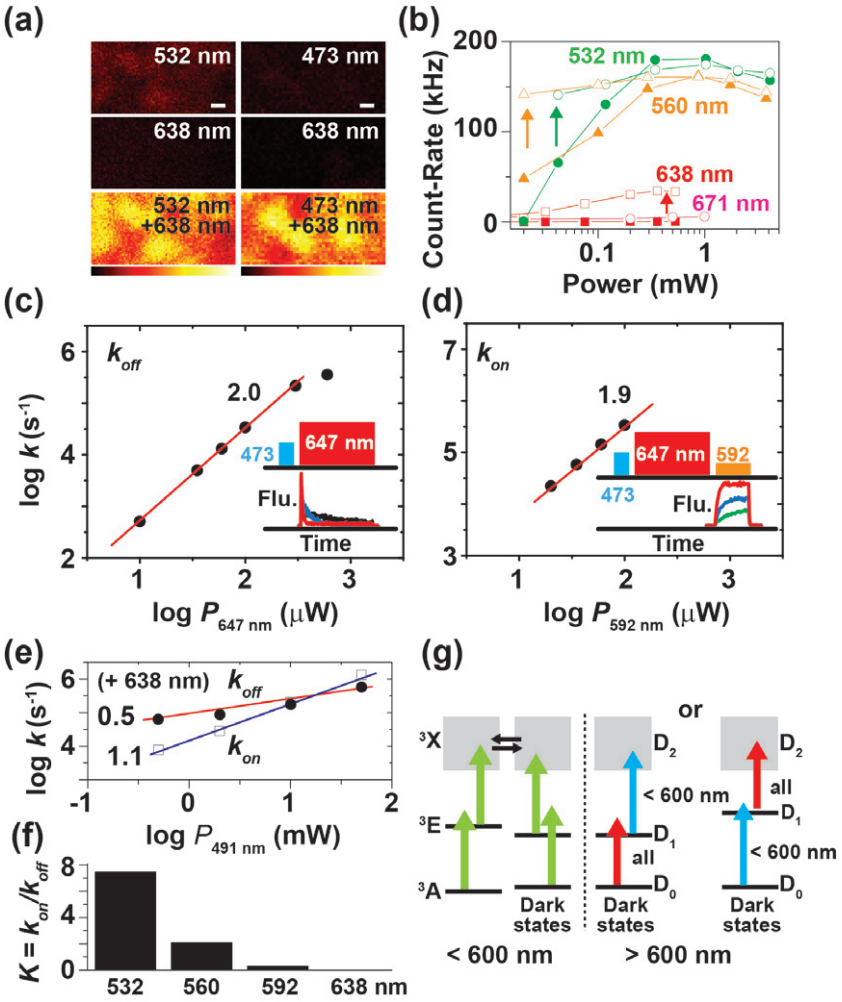

Figure 7. Photoswitching of NV fluorescence and the final electronic state model of NV fluorescence emission. (a) Scanning confocal fluorescence images of several nearby NV centres with sole CW excitation by 532 (9 μW, upper left), 473 (20 μW, upper right) and 638 nm light (200 μW, middle panels), and with simultaneous illumination by 532 and 638 nm (lower left) and 473 and 638 nm light (lower right). (b) Dependence of the fluorescence count rate on the power of the CW excitation light for different wavelengths with (open) and without (solid) addition of 1 mW of 473 nm light (arrows). (c), (d) Power dependence of $k_{\rm off}$ (c) and $k_{\rm on}$ (d) determined from the decays or increases of the fluorescence count rate over time of 50 000 pump–probe cycles (insets) during the 647 (c) and 592 nm (d) illumination, respectively. The numbers indicate the power of the dependence. (e) Dependence of $k_{\rm off}$ (black) and $k_{\rm on}$ (open) on the power of 491 nm CW light under simultaneous illumination with 638 nm light (200 μW) determined from autocorrelation fluorescence spectroscopy data. The numbers indicate the power of the dependence. (f) Wavelength dependence of the equilibrium constant $K = k_{\rm on}/k_{\rm off}$ between the dark and the bright state. (g) Final six-state model of NV centre fluorescence emission: whereas light of <600 nm can serve all transitions (green or blue arrows), light of >600 nm (red arrows) cannot serve one of the dark state transitions (either D_0–D_1 or D_1–D_2).

and also did not much improve emission following excitation at 671 nm, where stimulated emission is rather strong [20].

The photoswitching was further investigated by conducting pump–probe experiments applying 473, 647 and 592 nm excitation pulses. Figure 7(c) depicts a pump–probe scheme for the direct observation of off-switching by >600 nm light. A 20 μs-long pulse of 473 nm light prepares the NV centre for a maximum possible population of the ground (bright) triplet state. A subsequent 250 μs-long pulse of 647 nm light excites fluorescence and transfers the NV centre into the dark state, i.e. switches off fluorescence emission. Averaging the signal over 50 000 sweeps of the pump–probe cycles results in fluorescence decay during the 647 nm light illumination to a residual level given by background contributions due to, for example, Raman scattering. An exponential fit to this decay results in values of the (decay) rate k_{off} of off-switching by 647 nm light, as depicted in figure 7(c) for increasing power P_{647} of the 647 nm laser. Off-switching occurs within 3 μs with a power of only $P_{647} = 600\,\mu$W. Further, k_{off} increases with P_{647} in a strongly nonlinear manner, confirming our previous observations of an efficient dark state population by a two-step absorption process.

Figure 7(d) depicts a pump–probe scheme for the direct observation of on-switching by 592 nm light. Subsequent 20 and 100 μs-long pulses of 473 and 647 nm light prepare the NV centre for a maximum possible population of the dark state. A subsequent 80 μs-long pulse of 592 nm light excites fluorescence and partially transfers the NV centre back into its bright triplet state, i.e. it switches on fluorescence emission. Averaging the signal over 50 000 sweeps of the pump–probe cycles results in a fluorescence rise during the 592 nm light illumination and an exponential fit to these data at a rate k_{on} of on-switching by the 592 nm light. On-switching occurs within 3 μs with a power of $P_{592} = 300\,\mu$W of the 592 nm light. Further, k_{on} increases with P_{592} in a strongly nonlinear manner (figure 7(d)), confirming our previous observations of an efficient dark state de-population by <600 nm light via two-step absorption processes.

Figure 7(e) shows off- and on-switching rates k_{off} and k_{on} determined from fluorescence correlation data recorded for simultaneous illumination of 638 nm (200 μW) and increasing powers P_{491} of 491 nm light. The rather strong illumination by the 638 nm light already depopulates the bright state quite efficiently, resulting in a hardly increased off-switching k_{off} upon addition of 491 nm light. In contrast, the on-switching rate k_{on} increases linearly with power P_{491} of 491 nm light.

All of the above observations on photoswitching can be explained by our electronic state model. The equilibrium constant $K = k_{\mathrm{on}}/k_{\mathrm{off}}$ between dark and bright states decreases with increasing wavelength, reaching zero at long wavelengths (figure 7(f)). As a consequence, red light of >600 nm efficiently switches off the NV fluorescence by populating the dark state, while blue light <600 nm depopulates the dark state. Within the manifold of the three bright (^{3}A, ^{3}E and ^{3}X) and three dark state levels (D_0, D_1 and D_2), the low photon energy of >600 nm red light is larger than the $^3\mathrm{A} \rightarrow {}^3\mathrm{E}$ and $^3\mathrm{E} \rightarrow {}^3\mathrm{X}$ energy gaps. Thus, these photons efficiently depopulate the bright triplet state via ^{3}X, but their energy is too low to serve either the $D_0 \rightarrow D_1$ or the $D_1 \rightarrow D_2$ transition. In contrast, all four transitions are excited by photons of wavelengths <600 nm (figure 7(g)). This also gives an explanation for the observed linear dependence on the 491 nm laser power of figure 7(e) (when simultaneously applying strong 638 nm light). Saturating the accessible $D_0 \rightarrow D_1$ or $D_1 \rightarrow D_2$ transition by the 638 nm light, addition of increasing levels of the blue 491 nm light excites only the ($D_0 \rightarrow D_1$ or $D_1 \rightarrow D_2$) transition that is inaccessible to the red light, and therefore leads to a recovery of the bright fluorescent state via a one-photon process.

4. Discussion and conclusions

We have carried out power- and wavelength-dependent measurements of NV fluorescence emission and its fluctuations. All our observations indicate the strong involvement of a long-lived dark state and of several light-induced transitions, finally yielding the electronic state model of figure 7(g) as a suitable explanation. Our model includes the bright (triplet) state system with ground ^{3}A, first excited ^{3}E and higher excited ^{3}X electronic states, and a long-lived dark state comprising a ground D_0, a first excited D_1 and a higher excited D_2 electronic state. Crossing between the bright and dark states is most efficient between the highest excited states ^{3}X and D_2. This model explains the observed fluorescence count rate dependence on the excitation power, the squared dependence of the dark state population (k_{off}) and depopulation (k_{on}) rates on the excitation power, the decrease of the NV's fluorescence lifetime with excitation power, as well as the photoswitching characteristics of the NV emission (light >600 nm impedes fluorescence, while light <600 nm recovers it). The photophysical insights also allow us to improve the signal-to-background ratio of far-field fluorescence nanoscopy images of NV centres when applying pulsed instead of CW excitation.

In virtually all fluorescence experiments it is desired to maximize photon emission. In contrast to an ideal two-level system, such as a chromium colour centre in diamond [48], the photon emission of the NV centre is limited by the population of the dark states, requiring the minimization of the latter. From our results, we conclude that the most efficient depletion of the dark states and thus the highest achievable emission is achieved for wavelengths $\leqslant 532$ nm. The maximum achievable fluorescence signal is more or less similar following 473 or 532 nm excitation. Addition of 473 or 491 nm light to 532 nm excitation does not increase fluorescence emission further. The enhanced absorption cross-section of the 532 nm compared to the 473 nm only leads to a steeper increase of fluorescence with low laser power. Hence, fluorescence emission of NV centres is realized most effectively for moderate laser powers ($\sim 500\,\mu$W, i.e. 1.3 MW cm^{-2}) of 532 nm light.

Our observations gave insights into the number of electronic bright and dark states and their transitions involved in the fluorescence emission of NV centres. We do not claim that our proposed model is the ultimate model of the NV centre's electronic states; rather it gives a reasonable explanation for the dependence of the fluorescence emission on laser power and wavelength. We do not perform a specific assignment of the different states to electronic states proposed earlier in the literature (for example [29, 31]). For example, the exact nature of the dark state remains to be defined. A potential candidate may be the NV's singlet state. Several theoretical reports have suggested the existence of at least two singlet states with a calculated energy gap of 0.6–1.4 eV [49, 50]. However, this energy gap is lower than the photon energy of the red light. This implies that red light is able to excite these transitions and thus to depopulate the dark state, which does not match with our data. Another dark state candidate is a photo-ionized NV centre such as the neutral-charged NV^0 state [25, 26, 34]. Very recently, single-shot NMR measurements have identified the NV^0 as the long-lived dark state of NV^- fluorescence emission, which is furnished with extra electrons from nearby nitrogen atoms by green or blue excitation [25]. The photoionization level of nitrogen atoms (1.9 eV) in diamond is, however, below that of 600–640 nm light [51], implying that the red light should also photo excite the substitutional nitrogen. In contrast to NV^-–NV^0 photochromism detected in natural diamonds [8], we could (upon simultaneous illumination by blue and red light) not observe emission of NV^0 in the range of 600–640 nm [20]. One possible explanation may be that the red

light populates the NV^0 but cannot elicit its fluorescence emission, and addition of the blue light results in a quick recovery of NV^-, whose emission then dominates the fluorescence signal.

We conducted most of our experiments in synthetic type IIa diamond. Experiments in other material, especially with varying nitrogen and vacancy concentration, as well as the study of fluorescent NV nanodiamonds will further highlight the nature and characteristics of the dark state. Nevertheless, our observations and characterization of NV fluorescence signal give novel insights into the understanding of the NV centre's photon emission, and help to further optimize quantum optical [25, 26] and super-resolution microscopy experiments. For example, the insights into the optically driven reversible on–off switching of the NV centre's emission should not only improve the performance of deterministic-based super-resolution microscopy as, for example, presented in this paper for GSD microscopy [19, 20], but should also open up possibilities of using NV centre emission for stochastic single-molecule-based super-resolution microscopy such as (fluorescence) photoactivation localization microscopy [52, 53] or stochastic optical reconstruction microscopy [54].

Acknowledgments

We thank A Schönle for support with Imspector software and D Twitchen (Element 6) for providing the type IIa bulk diamond sample. Funding by the Volkswagen Foundation (to SWH) is gratefully acknowledged.

References

[1] Gruber A, Drabenstedt A, Tietz C, Fleury L, Wrachtrup J and von Borczyskowski C 1997 *Science* **276** 2012–4
[2] Jelezko F and Wrachtrup J 2006 *Phys. Status Solidi* a **203** 3207–25
[3] Balasubramanian G *et al* 2008 *Nature* **455** 648–51
[4] Maze J R *et al* 2008 *Nature* **455** 644–7
[5] Wrachtrup J and Jelezko F 2006 *J. Phys.: Condens. Matter* **18** S807–S24
[6] Davies G and Hamer M F 1976 *Proc. R. Soc. Lond.* A **348** 285–98
[7] Uedono A, Mori K, Morishita N, Itoh H, Tanigawa S, Fujii S and Shikata S 1999 *J. Phys.: Condens. Matter* **11** 4925–34
[8] Gaebel T *et al* 2006 *Appl. Phys.* B **82** 243–6
[9] Rondin L *et al* 2010 *Phys. Rev.* B **82** 115449
[10] Hauf M V *et al* 2011 *Phys. Rev.* B **83** 081304
[11] Loubser J and Vanwyk J A 1978 *Rep. Prog. Phys.* **41** 1201–48
[12] Jelezko F, Popa I, Gruber A, Tietz C, Wrachtrup J, Nizovtsev A and Kilin S 2002 *Appl. Phys. Lett.* **81** 2160–2
[13] Harrison J, Sellars M J and Manson N B 2004 *J. Lumin.* **107** 245–8
[14] Hell S W and Wichmann J 1994 *Opt. Lett.* **19** 780–2
[15] Hell S W 2007 *Science* **316** 1153–8
[16] Rittweger E, Han K Y, Irvine S E, Eggeling C and Hell S W 2009 *Nature Photon.* **3** 144–7
[17] Han K Y, Willig K I, Rittweger E, Jelezko F, Eggeling C and Hell S W 2009 *Nano Lett.* **9** 3323–9
[18] Wildanger D, Maze J and Hell S W 2011 *Phys. Rev. Lett.* **107** 017601
[19] Rittweger E, Wildanger D and Hell S W 2009 *Europhys. Lett.* **86** 14001
[20] Han K Y, Kim S K, Eggeling C and Hell S 2010 *Nano Lett.* **10** 3199–203
[21] Maurer P C *et al* 2010 *Nature Phys.* **6** 912–8
[22] Krueger A 2008 *Chem.—Eur. J.* **14** 1382–90

[23] Fu C C, Lee H Y, Chen K, Lim T S, Wu H Y, Lin P K, Wei P K, Tsao P H, Chang H C and Fann W 2007 *Proc. Natl Acad. Sci. USA* **104** 727–32
[24] Tzeng Y K, Faklaris O, Chang B M, Kuo Y M, Hsu J H and Chang H C 2011 *Angew. Chem. Int. Edn* **50** 2262–5
[25] Waldherr G, Beck J, Steiner M, Neumann P, Gali A, Frauenheim T, Jelezko F and Wrachtrup J 2011 *Phys. Rev. Lett.* **106** 157601
[26] Waldherr G, Neumann P, Huelga S F, Jelezko F and Wrachtrup J 2011 *Phys. Rev. Lett.* **107** 090401
[27] Drabenstedt A, Fleury L, Tietz C, Jelezko F, Kilin S, Nizovtzev A and Wrachtrup J 1999 *Phys. Rev.* B **60** 11503–8
[28] Kurtsiefer C, Mayer S, Zarda P and Weinfurter H 2000 *Phys. Rev. Lett.* **85** 290–3
[29] Rogers L J, Armstrong S, Sellars M J and Manson N B 2008 *New J. Phys.* **10** 103024
[30] Nizovtsev A P, Kilin S Y, Jelezko F, Popa I, Gruber A, Tietz C and Wrachtrup J 2003 *Opt. Spectrosc.* **94** 848–58
[31] Manson N B, Harrison J P and Sellars M J 2006 *Phys. Rev.* B **74** 104303
[32] Beveratos A, Brouri R, Poizat J P and Grangier P 2001 Bunching and antibunching from single NV color centers in diamond *Quantum Communication, Computing and Measurement* vol 3, ed P Tombesi and O Hirota (New York: Kluwer) pp 261–7
[33] Plakhotnik T and Chapman R 2011 *New J. Phys.* **13** 045001
[34] Robledo L, Bernien H, van Weperen I and Hanson R 2010 *Phys. Rev. Lett.* **105** 177403
[35] Meijer J, Stephan A, Adamczewski J, Röcken H, Weidenmüller U, Bukow H H and Rolfs C 1999 Microprobe as implanter for semiconductor devices *Nucl. Instrum. Methods Phys. Res.* **158** 3943
[36] Staudt T, Lang M C, Medda R, Engelhardt J and Hell S W 2007 *Microsc. Res. Tech.* **70** 1–9
[37] Brouri R, Beveratos A, Poizat J P and Grangier P 2000 *Opt. Lett.* **25** 1294–6
[38] Ringemann C, Schonle A, Giske A, von Middendorff C, Hell S W and Eggeling C 2008 *ChemPhysChem* **9** 612–24
[39] Gregor I, Patra D and Enderlein J 2005 *ChemPhysChem* **6** 164–70
[40] Eggeling C, Volkmer A and Seidel C A M 2005 *ChemPhysChem* **6** 791–804
[41] Abbe E 1873 *Arch. Mikrosk. Anatomie* **9** 413–68
[42] Hell S W 2004 *Phys. Lett.* A **326** 140–5
[43] Hofmann M, Eggeling C, Jakobs S and Hell S W 2005 *Proc. Natl Acad. Sci. USA* **102** 17565–9
[44] Brakemann T *et al* 2011 *Nature Biotechnol.* **29** 942–7
[45] Hell S W and Kroug M 1995 *Appl. Phys.* B **60** 495–7
[46] Bretschneider S, Eggeling C and Hell S W 2007 *Phys. Rev. Lett.* **98** 218103
[47] Kasha M 1950 *Faraday Discuss.* **9** 14–9
[48] Aharonovich I, Castelletto S, Simpson D A, Greentree A D and Prawer S 2010 *Phys. Rev.* A **81** 043813
[49] Delaney P, Greer J C and Larsson J A 2010 *Nano Lett.* **10** 610–4
[50] Ma Y C, Rohlfing M and Gali A 2010 *Phys. Rev.* B **81** 041204
[51] Heremans F J, Fuchs G D, Wang C F, Hanson R and Awschalom D D 2009 *Appl. Phys. Lett.* **94** 152102
[52] Betzig E, Patterson G H, Sougrat R, Lindwasser O W, Olenych S, Bonifacino J S, Davidson M W, Lippincott-Schwartz J and Hess H F 2006 *Science* **313** 1642–5
[53] Hess S T, Girirajan T P K and Mason M D 2006 *Biophys. J.* **91** 4258–72
[54] Rust M J, Bates M and Zhuang X W 2006 *Nature Methods* **3** 793–5